Investigation of physical image characteristics and phenomenon of edge enhancement by phase contrast using equipment typical for mammography

Asumi Yamazaki[a)]
Graduate School of Medical Sciences, Nagoya University, 1-1-20 Daikouminami, Higashi-Ku, Nagoya, Aichi, Japan 461-8673

Katsuhiro Ichikawa
Graduate School of Medical Science, Kanazawa University, 5-11-80 Kodatsuno, Kanazawa, Ishikawa, Japan 920-0942

Yoshie Kodera
School of Health Sciences, Nagoya University, 1-1-20 Daikouminami, Higashi-Ku, Nagoya, Aichi, Japan 461-8673

(Received 4 April 2007; revised 15 July 2008; accepted for publication 16 July 2008; published 23 October 2008)

A technique called phase contrast mammography (PCM) has only recently been applied in clinical examination. In this application, PCM images are acquired at a 1.75× magnification using an x-ray tube for clinical use, and then reduced to the real size of the object by image processing. The images showed enhanced object edges; reportedly, this enhancement occurred because of the refraction of x rays through a cylindrical object. The authors measured the physical image characteristics of PCM to compare the image characteristics of PCM with those of conventional mammography. More specifically, they measured the object-edge-response characteristics and the noise characteristics in the spatial frequency domain. The results revealed that the edge-response characteristics of PCM outperformed those of conventional mammography. In addition, the characteristics changed with the object-placement conditions and the object shapes. The noise characteristics of PCM were better than those of conventional mammography. Subsequently, to verify why object edges were enhanced in PCM images, the authors simulated image profiles that would be obtained if the x rays were refracted and totally reflected by using not only a cylindrical substance but also a planar substance as the object. So, they confirmed that the object edges in PCM images were enhanced because x rays were refracted irrespective of the object shapes. Further, they found that the edge enhancements depended on the object shapes and positions. It was also proposed that the larger magnification than 1.75 in the commercialized system might be more suitable for PCM. Finally, the authors investigated phase-contrast effects to breast tissues by the simulation and demonstrated that PCM would be helpful in the diagnoses of mammography. [DOI: 10.1118/1.2968091]

Key words: digital mammography, phase contrast, edge enhancement, image characteristics

I. INTRODUCTION

X rays travel in the form of electromagnetic waves. When they pass through objects, their waves undergo a phase shift. The phenomena such as diffraction, interference, and refraction are resulted from the phase shift. The image contrast caused by this phase shift is generally called phase contrast. Many researchers have investigated phase-contrast imaging and reported an improvement of sharpness of an image by using it.[1–16] Most of the research reported that the spatial coherence of x rays was essential to phase-contrast imaging.[1–10] Therefore, they used synchrotron-radiation sources and microfocus x-ray tubes as x-ray sources.[1–4,6,7] However, synchrotron-radiation sources are available only at restricted facilities, and x-ray outputs from microfocus x-ray tubes are extremely weak to be used as sources. It should be considered that x-ray tubes for clinical use radiate incoherent x rays because the sizes of the focal spots are finite and the distances between the focal spots and objects are not sufficiently large to ensure coherent x rays.[8,9] Wu *et al.* stated that focal spots smaller than 1 μm could maintain coherence, when the 20-keV x-ray beam was supposed with the distance of 0.6 m between the focal spot and objects.[8] Although Kotre *et al.* explored the application of phase-contrast imaging to mammography using an x-ray tube with the focal spot of 0.7 mm × 0.3 mm, separations more than 2 m between the focal spot and objects were required to ensure coherent x rays.[10] As a result of these impractical conditions, the clinical application of phase contrast imaging remained unrealized. Recently, however, a technique called phase contrast mammography (PCM) was applied in clinical examinations.[11] PCM made it possible to image phase contrast with incoherent x rays from an x-ray tube for clinical use. In the system, images are acquired with a 1.75× magnification and then reduced to the real size of the object by image processing.

Reportedly, PCM images have enhanced object edges and their sharpness is better than that of images obtained by conventional mammography.[11–14] It is considered that refraction and reflection could occur with incoherent x rays, although diffraction and interference hardly occurred.[11–16] So, it was reported that the phenomenon of edge enhancement in PCM is attributed to the refraction of x rays.[11–16] This statement was proved by calculations using the theory of refraction through only a cylindrical substance as the object.[11,15,16] Some research has evaluated the image characteristics of PCM quantitatively.[13,14] Nevertheless, although Gido *et al.* measured modulation transfer function (MTF), noise power spectrum (NPS), and noise equivalent quanta (NEQ) of a PCM system, the measurement of the MTF using a tungsten slit did not include phase-contrast effects.[13] Although Matsuo *et al.* reported an improvement of sharpness by phase-contrast imaging with a customized mammography system, the spectral analysis of these images by Fourier transformation may include the influences of not only the improvement of sharpness but also the granularity and structures of objects.[14] In this study, we first measured the response characteristics to object edges and the noise characteristics of PCM and compared them with the characteristics of conventional mammography. Although MTF measurement using an edge of a metal plate such as steel is a widely accepted method for measuring the response characteristics of an image detector,[17] we evaluated phase-contrast effects by similar methods using acrylic substances. Results by our methods could be compared with response characteristics measured by established methods. The noise characteristics were evaluated by measuring digital Wiener spectra, which are numerically equivalent to the NPS. One of the significant points of this study was to verify why object edges were enhanced in PCM images. Consequently, we simulated the image profiles that would be obtained if x rays were refracted and totally reflected at object edges. In the simulation, we used not only a cylindrical substance but also a planar substance as the object and changed object positions on the table. Although investigations as to phenomena of edge enhancements through a planar object in PCM radiography have not been reported yet, we verified that the enhancements were attributed to the refraction of x rays irrespective of the object shapes. Surprisingly, we found that phenomena of edge enhancements in PCM were characterized by the object shapes and the positional relation between the focal spot and the objects. We also investigated phase-contrast effects due to magnifications by radiography and the simulation. Further, as an ultimate objective of this study was to investigate phase-contrast effects to breast tissues, we did it by the simulation. The results showed that PCM would be helpful in the diagnosis of breast images.

II. MATERIALS AND METHODS

II.A. PCM system

The mammography equipment used was a Mermaid (model MGU-100B; Konica Minolta M&G, Inc., Tokyo, Japan). PCM radiography producing 1.75× magnified images and conventional mammography producing contact images can be performed with this equipment. The geometrical layouts of PCM radiography and conventional mammography are shown in Fig. 1. The nominal focal-spot sizes of PCM radiography and conventional mammography were 0.1 and 0.3 mm, respectively. Although a table without a bucky was used in PCM radiography, it must be changed to a table with a bucky for conventional mammography. The distance between each focal spot and the surface of each table is 650 mm. The distance between the surfaces of the table without a bucky and the image detector is 490 mm in PCM radiography. In this commercialized PCM system, photostimulable phosphor plates with a sampling pitch of 0.04375 mm are used as image detectors. The size of the plate for PCM radiography is 35 cm×43 cm and that for conventional mammography is 18 cm×24 cm. PCM images are reduced to the size of the contact images by image processing and printed with a 0.025-mm pitch on dry silver films. Contact images are printed with a 0.04375-mm pitch on the films.

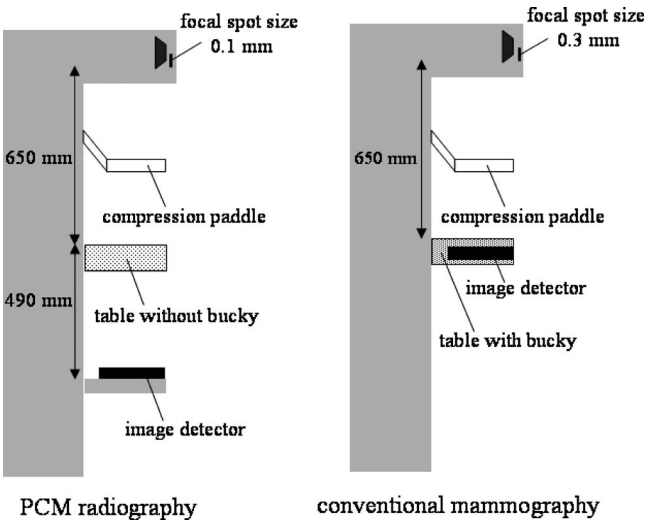

FIG. 1. Geometrical layouts of PCM radiography and conventional mammography.

II.B. MTFs and presampling MTFs

MTFs of a screen/film (S/F) system and presampling MTFs of a computed radiography (CR) system were measured by an edge method using a 0.1-mm thick tungsten edge, in order to analyze the first image characteristics of the image detectors used in this study.[17] For measuring MTFs of the S/F system and presampling MTFs of the CR system for conventional mammography, image detectors were set on the table with a bucky, as shown in the layout in the right panel of Fig. 1, and the tungsten edge was set on each image detector. For measuring presampling MTFs of the CR system for PCM, the tungsten edge was set on the image detector, as shown in the left panel of Fig. 1. The tungsten edges were placed in the four directions shown in Fig. 2. The arrows in Fig. 2 at a position 5 cm from the center of the chest wall side of the table show lines and directions of data used for

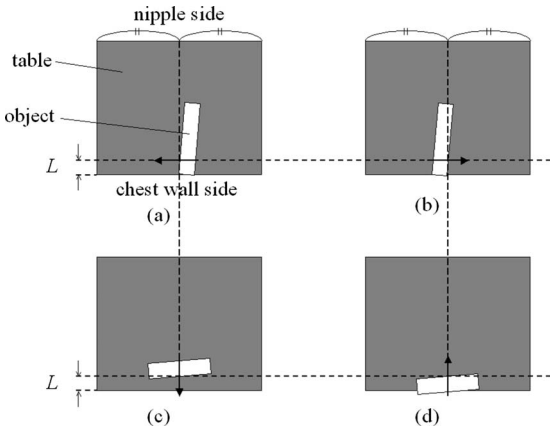

FIG. 2. Placement directions of objects. The object edges were placed on the right (a) or left (b) relative to the center of the table, or placed behind (c) or in front (d) at a distance L from the chest wall side of the table. The arrows show lines and directions used for measuring MTFs and response functions. L is 5 cm in the MTF measurements and 1 cm in the response function measurements. The edges were tilted by angles between 1.5° and 3° relative to the long or short axis of the table.

calculating MTFs and presampling MTFs. Exposures were performed at 28 kV with a molybdenum anode in combination with a molybdenum-added filter (0.03-mm thickness) attached to the equipment. An aluminum-added filter (2-mm thickness) was also attached to approximate the beam quality to the quality after transmission through a breast tissue. A S/F system (MD-100/CM-H; Konica Minolta M&G Inc., Tokyo, Japan) and photostimulable phosphor plates for PCM and conventional mammography (RP-5M110PCM, RP6M110; Konica Minolta M&G, Inc., Tokyo, Japan) were used as image detectors. Exposure levels for measurements of MTFs of the S/F system were 32 mA s, and the air kerma at the surface of the image detector was 0.19 mGy. Exposure levels for measurements of presampling MTFs of the CR system were 100 mA s, and the air kermas at the surfaces of the image detectors for PCM and conventional mammography were 0.18 and 0.6 mGy, respectively. The exposed films in the S/F system were developed with an automatic film processor (TCX-202; Konica Minolta M&G, Inc., Tokyo, Japan) in 90 s per cycle at 32° using TD-202 (Konica Minolta M&G, Inc., Tokyo, Japan) as the developer and TF-202 (Konica Minolta M&G, Inc., Tokyo, Japan) as the fixer. The films were digitized by a high-resolution single-lens reflex-type digital camera (D70; Nikon Co., Tokyo, Japan). Ichikawa *et al.* measured the image characteristics of liquid crystal displays using a similar digital camera, and they demonstrated that the spatial resolution of the camera was sufficient to measure MTFs of objects.[18–22] The camera has charge coupled device (CCD), sensor arrays of 3008×2000 and a contrast resolution of 14 bits. The sampling pitch of the camera is about 0.08 mm on the plane of the film if the lens is adjusted with the highest magnification. We verified that the spatial resolutions in the horizontal and vertical directions of the digital camera were the same. The photostimulable phosphor plates were scanned at a sampling pitch of 0.04375 mm by a CR reader (REGIUS Vstage model 190; Konica Minolta M&G, Inc., Tokyo, Japan). Note that the main scanning direction of the plate for PCM radiography corresponds to the direction shown by the arrows (c) and (d) in Fig. 2. On the other hand, the main scanning direction of the plate for conventional mammography corresponds to the directions (a) and (b). The subscanning direction of each plate is perpendicular to the main scanning direction.

Raw data of images acquired from the digital camera and CR reader were used for the calculations. Optical densities of the digitized films could be determined under the assumption that the intensity of the incident light to the camera was proportional to the pixel values of the raw data acquired from the camera. From the data on the lines on the tungsten edge shown by the arrows in Fig. 2, we obtained profiles of optical densities of the S/F system and pixel values of the CR system. The profiles were averaged so that the influences of noise were removed. Because the tungsten edge was tilted and the profile data were projected onto the axis perpendicular to the edge, the data were obtained with pitches smaller than the sampling pitches of the digital camera and the photostimulable phosphor plates. Edge spread functions (ESFs) were obtained by transforming the profiles into x-ray intensities. MTFs were calculated by the Fourier transformation of differentiated data of ESFs. Each modulation transfer factor was normalized with a factor whose spatial frequency was zero. Presampling MTFs for PCM were adjusted by multiplying the spatial frequency by 1.75 and convolving the square wave of the focal-spot size so that the image size became equal to the contact image size and the influences of the focal-spot blurring were included.

II.C. Object-edge-response characteristics

The response characteristics to object edges in the spatial frequency domain of PCM and conventional mammography were measured by calculating response functions. The objects used were an acrylic plate (2-mm thickness) and an acrylic rod (2-mm diameter) in air or an acrylic box filled with salad oil. Image detectors used were the S/F system and photostimulable phosphor plates used for measuring MTFs and presampling MTFs. We obtained images, as shown in the layouts in Fig. 1, by setting the objects on the table. In conventional mammography, however, image detectors were set on the table with a bucky and the objects were set on image detectors. The acrylic plate and acrylic rod were placed in four different directions, as shown in Fig. 2. Data for a position 1 cm from the center of the chest wall side of the table, shown by arrows in Fig. 2, were used for calculating response functions. Exposures were performed under the conditions shown in Table I. The beam quality was same as that for measuring MTFs and presampling MTFs. Although exposure levels and the air kermas at the surfaces of the image detectors are shown in Table I, note that the air kermas differed, even if outputs (exposure levels) of the x rays were same. This is because focus image distances (FIDs) in PCM and conventional mammography differed.

The flowchart for the measurements of the edge-response characteristics is shown in Fig. 3. We calculated response

TABLE I. Exposure conditions for measurements of edge-response characteristics.

Detector	Object (placement direction in Fig. 2)	Tube voltage (anode/ added filtration in the equipment) +added filtration	Exposure level (mAs) [Air kerma (mGy)]	
			PCM	conventional mammography
S/F	Acrylic plate in air (a), (b), (c), (d)	28 kV (molybdenum/ 0.3-mm molybdenum) + 2-mm aluminum	100 (0.18)	32 (0.19)
	Acrylic rod in air (a), (b), (c), (d)			
	Acrylic plate in oil (a)		200 (0.35)	40 (0.24)
CR	Acrylic plate in air (a), (b), (c), (d)		100 (0.18)	100 (0.60)
	Acrylic rod in air (a), (b), (c), (d)			

functions by the same method as that used for the calculation of MTFs. The exposed films in the S/F system were developed and then digitized by using the digital camera. The photostimulable phosphor plates were scanned by the CR reader. From raw data of the images acquired, the profiles of the edge of objects were obtained. The profile data were averaged and transformed into x-ray intensities. The response functions were calculated by the Fourier transformation of differentiated data of x-ray intensities of profiles. Each response factor was normalized with a response factor whose spatial frequency was zero. The response functions of PCM were adjusted by multiplying the spatial frequency by 1.75 so that the image size became equal to the contact image size.

II.D. Noise characteristics

The noise characteristics of the CR system for PCM and conventional mammography in the spatial frequency domain were measured by obtaining digital Wiener spectra. Exposures were performed similar to the layouts shown in Fig. 1 to obtain uniformly exposed images; for this, photostimu-

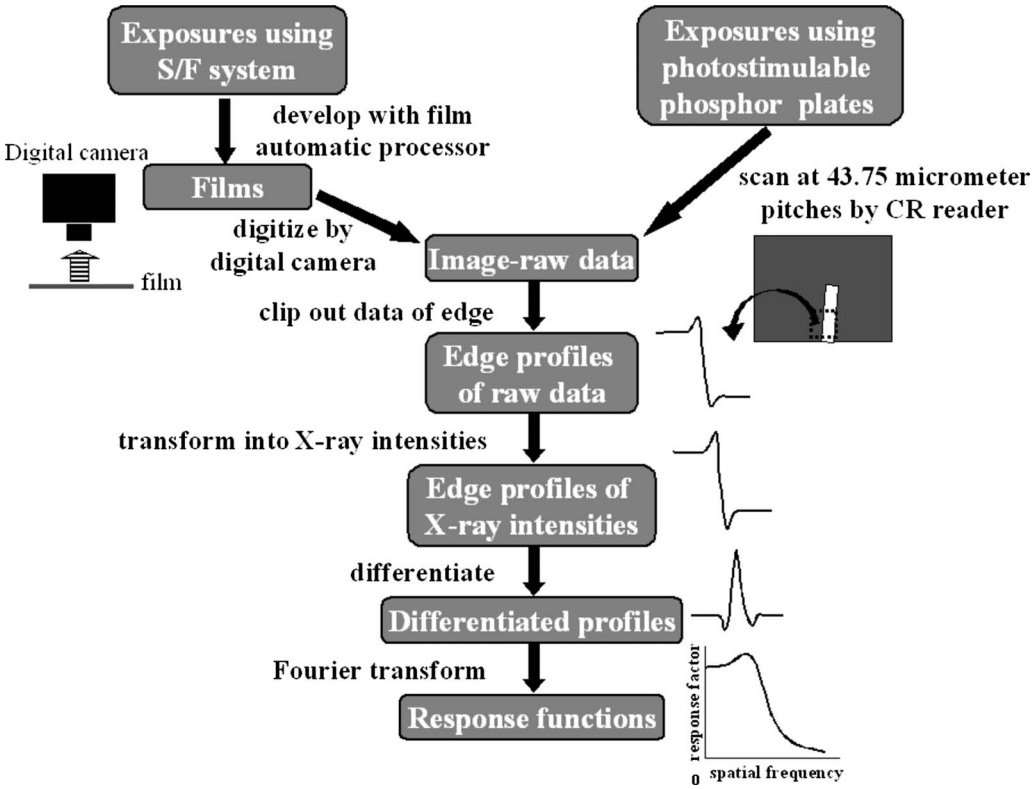

FIG. 3. Flowchart depicting the measurement of edge-response characteristics.

lable phosphor plates were used as image detectors. The beam quality was same as that in the measurements of MTFs and response characteristics. In the layouts of both PCM radiography and conventional mammography, the exposure levels were 25, 50, and 100 mA s, which corresponded to 0.04, 0.09, and 0.18 mGy (air kerma at the surface of the image detector for PCM), respectively, and 0.15, 0.30, and 0.60 mGy (air kerma at the surface of the image detector for conventional mammography), respectively.

Raw data of exposed images in the region of interest (ROI) of 5 cm × 5 cm around a position 5 cm from the center of the chest wall side of the table were used for calculating digital Wiener spectra. The calculation was performed using a method of two-dimensional Fourier transformation according to IEC 62220-1-2.[17] Raw data in the ROI were transformed into x-ray intensities. Trend removal was performed by fitting a two-dimensional second-order polynomial. Although the pixel pitch of the raw data in PCM images was the same (0.043 75 mm) as that of conventional mammography images, because the PCM images were printed with a 0.025-mm pitch in dry silver films, Wiener spectral values for PCM were divided by the square of the magnification (1.75) and the spatial frequency of Wiener spectra for PCM was adjusted by multiplication with 1.75.

II.E. Simulation based on refraction of X rays

II.E.1. Details of the simulation

To investigate why object edges were enhanced in PCM images, we simulated image profiles that would be obtained if the behavior of x rays had followed the theories of refraction and total reflection. Diffraction and interference were not included since x-ray tubes for mammography generated incoherent x rays because of the restrictions of focal spot sizes and geometrical conditions as described in Sec. I. The simulation was performed on the same geometrical layout as that of the PCM radiography shown in Fig. 1 using an acrylic plate of 2-mm thickness and an acrylic rod of 2-mm diameter as the objects. The size of a focal spot was 0.1 mm. The object edges were positioned on the table and these positions could be shifted within a range of 70 mm to the right and left from the position just under the center of the focal spot. Attenuation, refraction based on Snell's law, and total reflection of x rays were calculated under the assumption of monochromatic x rays whose energies were 14, 15.5, 17.4, and 19.6 keV. The effective energy of the polychromatic spectrum of 28 kV with a molybdenum anode in combination with a molybdenum inherent filter was 15.5 keV on the condition without any absorber by the equipment used in this study. The values 17.4 and 19.6 keV are characteristic x rays of molybdenum. Attenuation was calculated using Eq. (1),

$$I = I_0 \cdot \exp(-\mu \cdot x), \tag{1}$$

where I is the intensity of x rays after they pass through a medium whose linear attenuation coefficient is μ and thickness is x, and I_0 is the intensity of x rays before they pass through the medium. The refractive index n of x rays in the medium is defined as

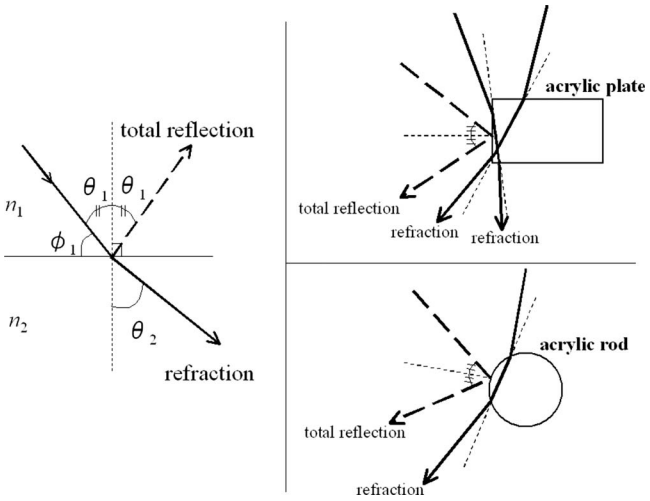

FIG. 4. The model of x-ray behaviors with refraction and total reflection. The left panel shows the general model of the behavior. The upper right panel shows the model with an acrylic plate, and the lower right panel shows that with an acrylic rod.

$$n = 1 - \delta - i\beta, \tag{2}$$

$$\delta = Na\frac{Z}{A}\rho e^2\lambda^2/(2\pi mc^2), \tag{3}$$

$$\beta = \mu\lambda/4\pi, \tag{4}$$

where i is an imaginary unit; Na is Avogadro's number (6.02×10^{23}); Z is the atomic number; A is the nuclear number; ρ is the density (g/cm^3) of the medium; $e^2/(mc^2)$ is the classical radius of an electron (2.82×10^{-13} cm); λ is the wavelength (cm) of the x rays; and μ is the linear attenuation coefficient (cm^{-1}) of the medium.[1,8,23] Because Z/A can be regarded as 0.5 in many atoms, the approximate value of δ is determined by the density and wavelength. We calculated δ from the density of the acrylic substance or air and the wavelength of the x rays. Although β was calculated by the linear attenuation coefficient of air or the acrylic substance and the wavelength, β was much smaller than δ. The difference between β and δ was three figures. Therefore, we regarded β to be zero. Finally, n of air was determined as 0.999 999 998 96 and n of the acrylic substance was determined as 0.999 998 965 4, when the energy of x rays was assumed as 15.5 keV.

Reflectance and transmissivity of x rays were calculated approximately from the Fresnel coefficient.[24] Figure 4 shows the model of x-ray behavior with refraction and total reflection. In this model, it was assumed that x rays enter a medium with refractive index n_2 from a medium with refractive index n_1 at an incident angle θ_1. The angle φ_1 was defined as $\pi/2 - \theta_1$. The angle φ_c was defined from the critical angle as

$$\phi_c = \frac{\pi}{2} - \arcsin\left(\frac{n_2}{n_1}\right). \tag{5}$$

The reflectance r of x rays is defined as

$$r = \frac{(\phi_1 - A)^2 + B^2}{(\phi_1 + A)^2 + B^2}, \tag{6}$$

$$A = \frac{1}{\sqrt{2}}\{[(\phi_1^2 - \phi_c^2)^2 + 4\beta^2]^{1/2} + (\phi_1^2 - \phi_c^2)\}^{1/2}, \tag{7}$$

$$B = \frac{1}{\sqrt{2}}\{[(\phi_1^2 - \phi_c^2)^2 + 4\beta^2]^{1/2} - (\phi_1^2 - \phi_c^2)\}^{1/2}. \tag{8}$$

The transmissivity t of x rays was defined as

$$t = 1 - r. \tag{9}$$

X rays that reached the surface of the acrylic substance were refracted and reflected according to the probability of reflectance and transmissivity. If the x rays were refracted, their behavior followed Snell's law. According to Snell's law, the refracting angle θ_2 is defined as

$$\theta_2 = \arcsin\left(\sin\theta_1 \cdot \frac{n_1}{n_2}\right). \tag{10}$$

If the x rays were reflected, the reflex angle was equal to the incident angle.

The number of photons that arrived at the image detector under the above conditions was counted at a pitch of 0.0098 mm so that profiles were obtained. To contain the influences of the blur by the image detector, the profiles were convolved with the blurring function, which is equal to the line spread function (LSF) of the S/F system.

II.E.2. Comparison with profiles obtained by radiography

To compare profiles obtained by the simulation with those obtained by radiography, we obtained images of the acrylic plate of 2-mm thickness and acrylic rod of 2-mm diameter in the layout of PCM radiography shown in Fig. 1, changing the object positions on the table gradually within a range of 70 mm to the right and left from the position just under the center of the focal spot. The position just under the center of the focal spot was defined by the point where x rays entered the objects vertically. This point was 3 mm to the left from the center of the table shown in Fig. 2. The edges of the objects were positioned parallel to the short axis of the table. The conditions of exposure were 100 mA s with the same beam quality as that in the measurement of MTFs and response characteristics. The image detector used was the S/F system. Acquisitions of profiles transformed into x-ray intensities were performed by the same way as that used in measurements of MTFs in the S/F system.

II.F. Phase-contrast effect due to magnification

Although PCM images are acquired with a 1.75× magnification in the commercialized system, we investigated phase-contrast effects with several magnifications by radiography and the simulation described in Sec. II E 1.

II.F.1. Investigations by radiography

We put the acrylic plate of 2-mm thickness on the compression paddle in the layouts of the left panel of Fig. 1. PCM images were acquired with several magnifications between 1.75 and 2.6, as the height of the compression paddle was changed. The photostimulable phosphor plate for PCM in the CR system was used as the image detector. The FID was fixed as 1140 mm. We also acquired contact images setting the acrylic plate on the photostimulable phosphor plate for conventional mammography put on the table in the layouts of the right panel of Fig. 1. The edge of the acrylic plate was positioned at 10 mm to the right from the position just under the center of the focal spot and was tilted by about 2° relative to the short axis of the compression paddle. Exposures were performed at 100 mA s with the same beam quality as that in the measurement of MTFs. We obtained edge profiles and response functions from the images by the same way as that described in Sec. II C.

II.F.2. Investigations by the simulation

Edge profiles were calculated with magnifications between 1.75 and 4.5 using the simulation described in Sec. II E 1, although we could not set up the magnification more than 2.6 in radiography due to the geometric restriction. The geometrical layout was same as that of the left panel shown in Fig. 1. The FID was fixed. We used the acrylic plate of 2-mm thickness and the acrylic rod of 2-mm diameter in air as the objects. The positions of the objects were assumed as 10 mm to the right from the position just under the center of the focal spot. The simulation was also performed with the magnification 1.0 in the layouts of conventional mammography of Fig. 1. The energy of x rays was assumed as 15.5 keV. Profiles were obtained from the counts of the number of photons that arrived at the image detector at a pitch of 0.0023 mm. The profiles by the conditions of PCM were convolved with the LSFs of the CR system for PCM, and those by the conditions of conventional mammography were done with LSFs of the system for conventional mammography. We obtained response functions from the profiles.

II.G. Phase-contrast effect to breast tissue

We investigated phase-contrast effects to mammary glands in adipose tissue, which were ultimate objective of this study, with the simulation described previously. The geometrical layout was same as that of the PCM radiography shown in Fig. 1. Besides, the simulation on the layout of conventional mammography was also performed for reference. Table II shows densities, refractive indexes calculated by Eq. (2) and linear attenuation coefficients of breast tissues at 20 keV.[25] We simulated by the refractive indexes and linear attenuation coefficients of mammary glands and adipose tissue. We assumed models of mammary glands as planar forms (0.2-, 0.5-, 1-, 2-, 3-, and 5-mm thickness) and cylindrical forms (0.2-, 0.5-, 1-, 2-, 3-, and 5-mm diameter) for simplifying calculation. The edges of mammary glands were positioned on the table at 10 mm to the right from the posi-

TABLE II. Densities, refractive indexes, and linear attenuation coefficients of breast tissues at 20 keV.

	Density ρ (g/cm^3)	Refractive index n	Linear attenuation μ (cm^{-1})
Adipose tissue	0.930	0.999 999 514	0.45
Mammary gland	1.035	0.999 999 460	0.80
Breast carcinoma	1.045	0.999 999 454	0.85
Calcification	2.20	0.999 998 851	12.5

tion just under the center of the focal spot. The number of photons that arrived at the image detector was counted at a pitch of 0.0098 mm so that profiles were obtained. The profiles were convolved with the LSF of the S/F system by the same way as that of Sec. II F. We calculated response functions from the profiles by the same way as that described in Sec. II C.

III. Results

III.A. MTFs and presampling MTFs

Figure 5 shows MTFs of the S/F system. Figure 6 shows presampling MTFs of the CR system for PCM and conventional mammography. The letters (a), (b), (c), and (d) in these figures correspond to the directions in which the tungsten edge was placed, as shown in Fig. 2. MTFs of the S/F system in directions (a) and (b) were higher than those in directions (c) and (d). Although presampling MTFs of the CR system for PCM in directions (a) and (b) were higher than those in directions (c) and (d), opposite results were obtained in the system for conventional mammography. The directions (a) and (b) in the CR system for PCM correspond to a subscanning direction of the photostimulable phosphor plates, and the directions (c) and (d) correspond to the main scanning direction of the plates. On the other hand, the directions (a) and (b) in the system for conventional mammography correspond to the main scanning direction of the plates, and the directions (c) and (d) correspond to the subscanning direction of the plates. So, presampling MTFs in the subscanning direction were higher than those in the main scanning direction in both PCM and conventional mammography. Although presampling MTFs of the CR system for PCM were lower than those for conventional mammography without adjusting the spatial frequency, those for PCM were higher than those for the conventional mammography as a result of the adjustment, that is, because of the reduction of the magnified images.

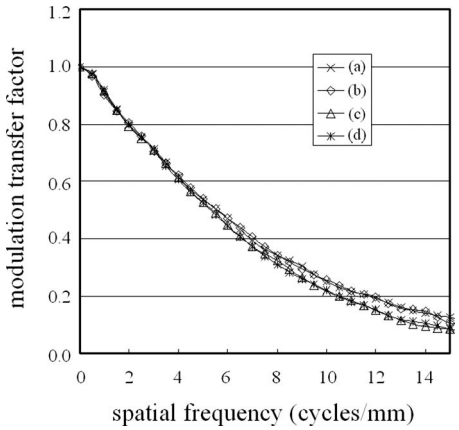

FIG. 5. MTFs of the S/F system.

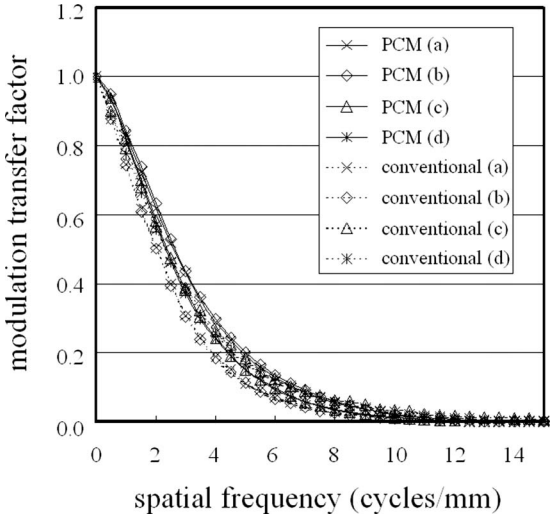

FIG. 6. Presampling MTFs of the CR system for PCM and conventional mammography.

III.B. Object-edge-response characteristics

Figure 7 shows the response functions and profiles at the object edges of PCM in the S/F system using the acrylic plate as the object. The profiles along the lines shown by arrows in the right panel are displayed. These profiles were transformed into x-ray intensities. Although the profiles at the edges of the acrylic plate were enhanced in all placement directions of the object, edge enhancements of the profiles in directions (a) and (b) were remarkable as compared with those in directions (c) and (d). Further, response functions in (a) and (b) were higher than those in (c) and (d).

Figure 8 shows the response functions and profiles at the object edges of PCM in the CR system using the acrylic plate as the object. The profiles were also transformed into x-ray intensities. Edge enhancements were detected on either the upper or lower side of the profiles in the subscanning direction of the photostimulable phosphor plates. In the main scanning direction of the plates, edge enhancements were hardly detected. The response functions in the subscanning direction were higher than those in the main scanning direction. In addition, a difference between the response functions in (a) and (b) in the subscanning direction appeared.

Figure 9 shows the response functions of PCM or conventional mammography in the S/F system or the CR system using the acrylic plate in the placement direction (a) in air or oil as the object. Response functions of PCM were higher than those of conventional mammography. Response functions in the S/F system were higher than those in the CR

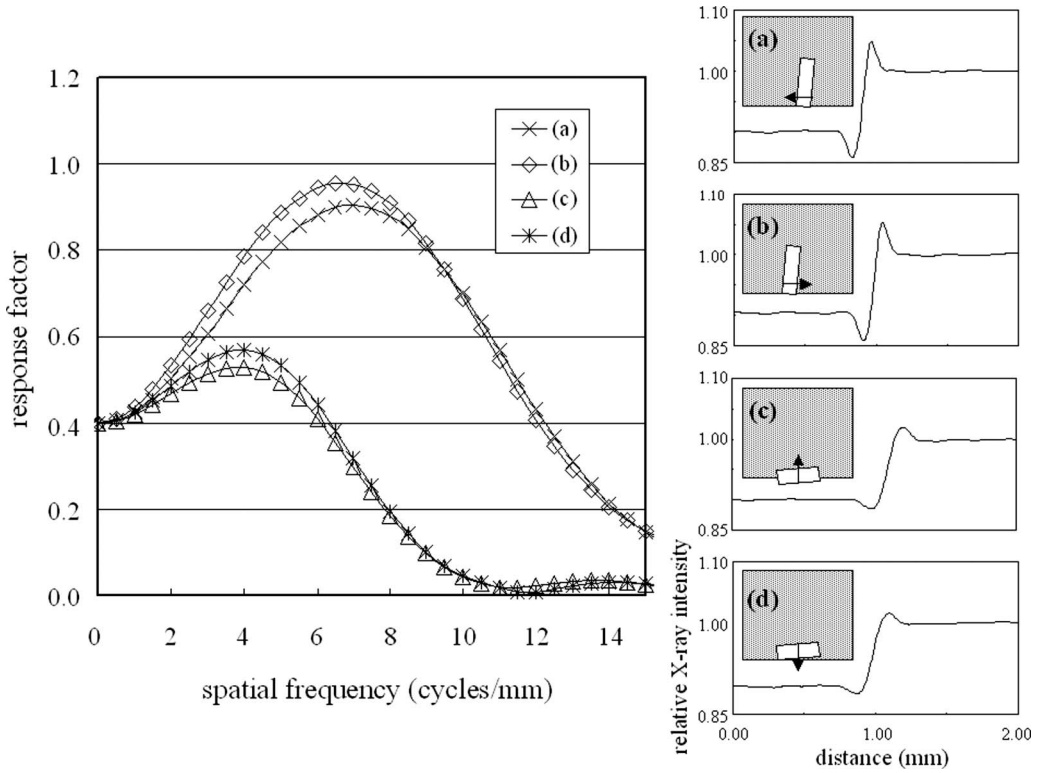

FIG. 7. Response functions and profiles at object edges in PCM in the S/F system using an acrylic plate as the object.

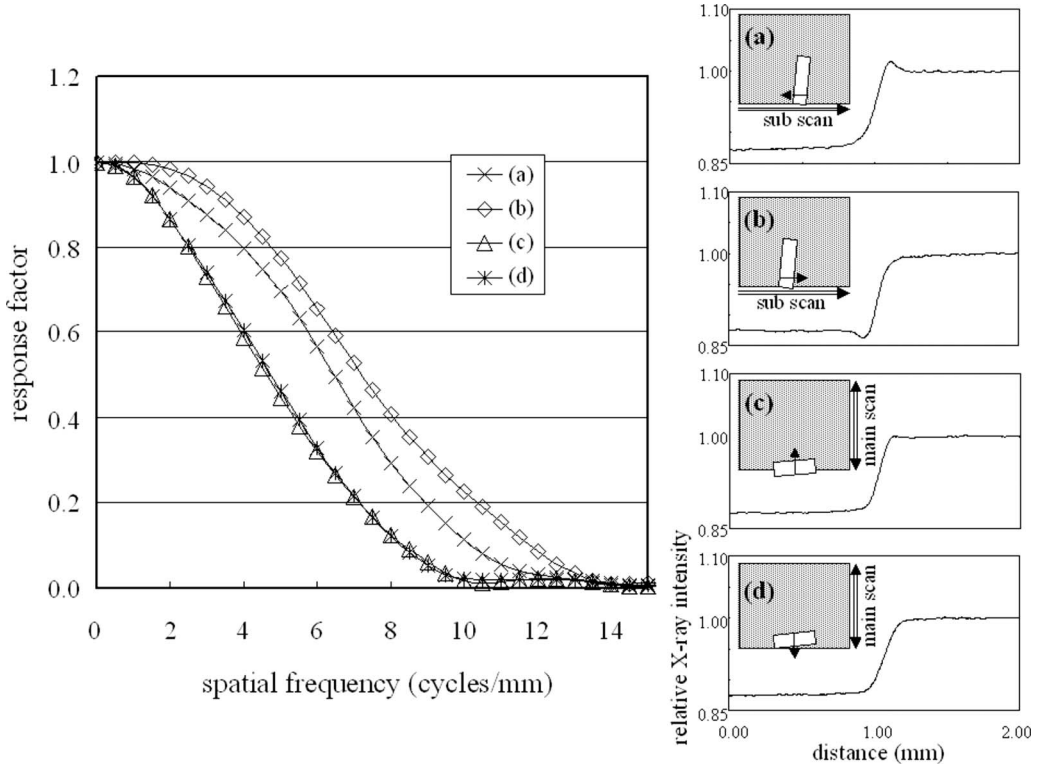

FIG. 8. Response functions and edge profiles of the object in PCM in the CR system using an acrylic plate as the object.

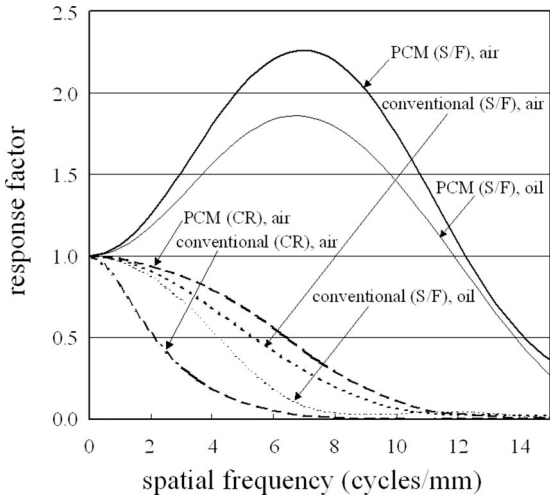

FIG. 9. Response functions of PCM or conventional mammography in the S/F system or CR system using an acrylic plate in air or oil as the object.

system. In the cases of response functions in the directions (b), (c), and (d), these tendencies were similar. The response functions using the acrylic plate in air were higher than those in oil.

Figure 10 shows the response functions of PCM or conventional mammography in the S/F system using the acrylic plate or acrylic rod in the placement direction (a) as the object. Figure 11 shows the profile at the edge of the acrylic rod in the direction (a) of PCM in the S/F system. The edge enhancement on the profile of the acrylic rod was not more remarkable than that of the acrylic plate, as shown in Figs. 7 and 11. The response functions using the acrylic plate were higher than those using the acrylic rod. However, even if the acrylic rod was used as the object, the response functions of PCM were higher than those of conventional mammography in the range of spatial frequencies higher than about 3 cycles/mm. These tendencies were the same as those in the CR system and in the placement directions (b), (c), and (d).

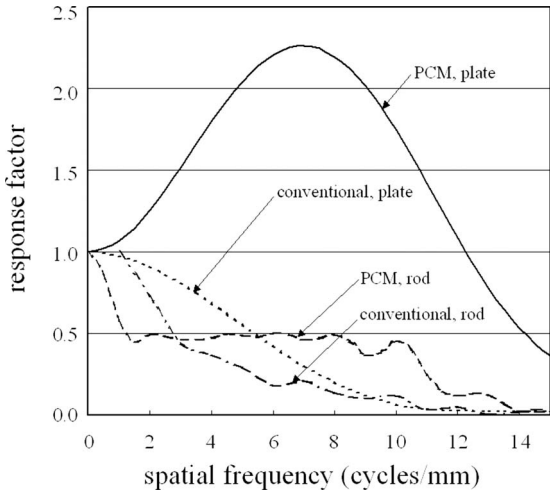

FIG. 10. Response functions of PCM or conventional mammography in the S/F system using an acrylic plate or acrylic rod.

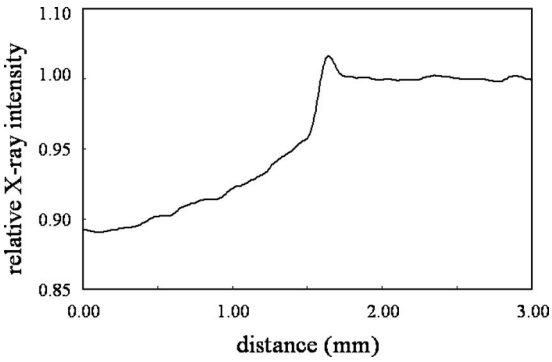

FIG. 11. Profile at the edge of an acrylic rod in PCM in the S/F system. Scale of the horizontal axis corresponds not with the size of the real object but rather with the size of the magnified object.

III.C. Noise characteristics

Figures 12 and 13 show digital Wiener spectra of the CR system for PCM and conventional mammography at 50 mA s in the main and subscanning directions, respectively. Digital Wiener spectra for PCM were lower than those of conventional mammography in both the main and subscanning directions. The same tendencies were observed at 25 and 100 mA s.

III.D. Comparison of simulation with radiography

Figures 14 and 15 show profiles obtained by the simulation with x rays of 15.5 keV using the acrylic plate and acrylic rod. The scale of the horizontal axis in these figures does not correspond with the size of a real object but rather the size of the magnified object. When the acrylic plate was set just under the center of the focal spot, the edge of the profile was hardly enhanced. If the acrylic plate was moved to the right and left, edge enhancements were detected on profiles at the edge positions. The intensities of the enhancements were maximum when the distance moved was about 10 mm. Even if the energy of the x rays was changed, similar profiles were obtained; in other words, intensities of edge enhancements changed according to the object position. However, intensities at the same object position were greater

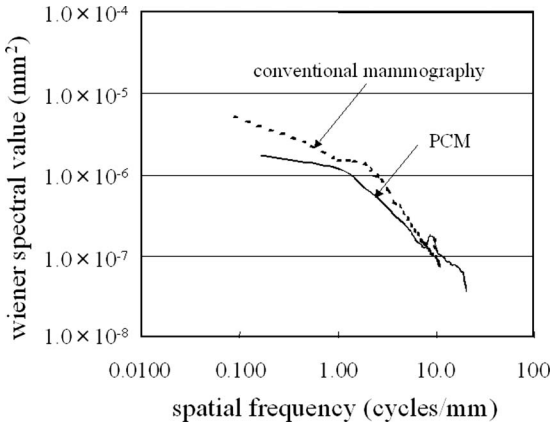

FIG. 12. Digital Wiener spectra in the main scanning direction.

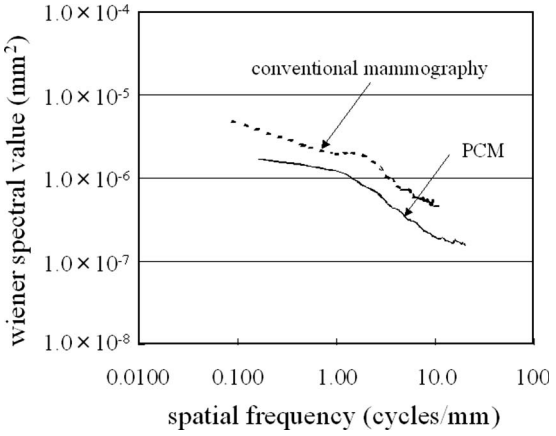

FIG. 13. Digital Wiener spectra in the subscanning direction.

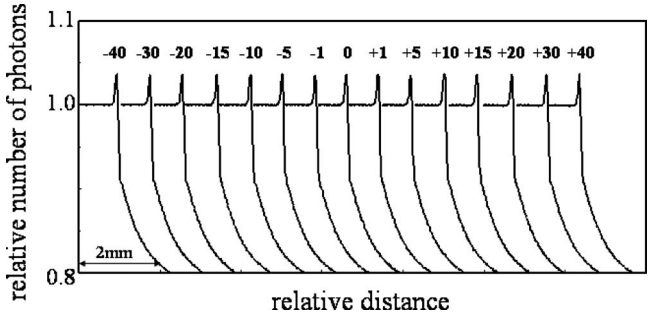

FIG. 15. Profiles obtained by the simulation with 15.5-keV x rays using an acrylic rod. The edge of the acrylic rod was positioned at −40, −30, −20, −15, −10, −5, −1, 0, +1, +5, +10, +15, +20, +30, and +40 mm to the right of the position just under the center of the focal spot.

with lower-energy x rays. When the acrylic rod was used as the object, even if the position of the object was changed, the intensities of edge enhancements hardly changed. Even if the energy of x rays was changed, similar profiles, in which the intensities of edge enhancements hardly changed due to the object position, were obtained. At the same time, we observed the similar tendency, wherein the intensities were greater with lower-energy x rays, to that with the acrylic plate.

Profiles obtained by radiography using the acrylic plate and acrylic rod are shown in Figs. 16 and 17, respectively. The scale of the horizontal axis in these figures corresponds with the size of the magnified object. In the profiles using the acrylic plate, the intensities of edge enhancements changed due to the object position and they were minimum at a position just under the center of the focal spot. The intensities were maximum if the object was moved about 10 mm from the position just under the center of the focal spot. The forms of the profiles using the acrylic rod hardly changed, irrespective of the object position.

III.E. Phase-contrast effect due to magnification

Figure 18 shows profiles by radiography in the CR system using the acrylic plate with several magnifications. The scale of the horizontal axis corresponds with the sizes of the objects projected on the image detectors. Although the edge profile with the magnification 1.0 was not enhanced, the intensity of the edge enhancement was larger as the magnification was increased. Figure 19 shows response functions calculated from profiles in Fig. 18. As the magnification was increased, the peak of the response function was also increased. Figures 20 and 21 show profiles and response functions by the simulation using the acrylic plate with several magnifications, respectively. The edge enhancement of the profile resulted in maximum intensity when the magnification was 2.8 or 3.0. The peak of the response function was maximum with the magnification 2.8. Figures 22 and 23 show profiles and response functions by the simulation using the acrylic rod, respectively. As the magnification was increased, intensities of the edge enhancements were increased in the range of the magnification less than 4.0. Intensity of the edge enhancement with the magnification 4.5 was almost equivalent to that with 4.0. The peak of the response function was maximum when the magnification was 3.0 or 4.0. The peak of the response function with the magnification 4.5 was lower than that with 4.0.

III.F. Phase-contrast effect to breast tissue

Figures 24 and 25 show profiles of planar and cylindrical mammary-gland edges acquired at a 0.0098-mm pitch by the simulation on the layout of PCM, respectively. The scales of

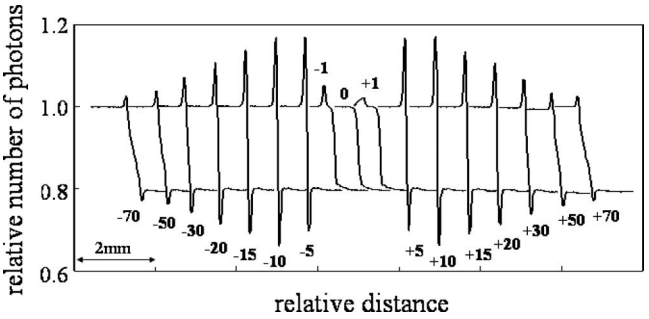

FIG. 14. Profiles obtained by the simulation with 15.5-keV x rays using an acrylic plate. The edge of the acrylic plate was positioned at −70, −50, −30, −20, −15, −10, −5, −1, 0, +1, +5, +10, +15, +20, +30, +50, and +70 mm to the right of the position just under the center of the focal spot.

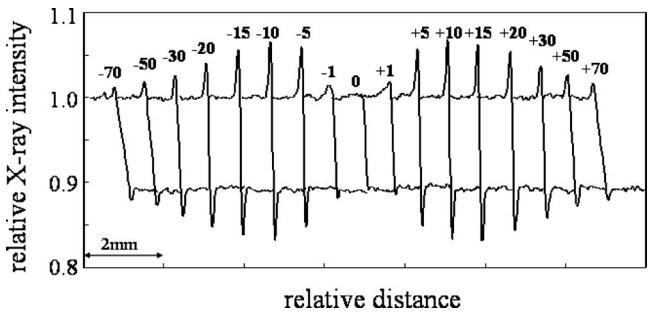

FIG. 16. Profiles obtained by radiography using an acrylic plate. The edge of the acrylic plate was positioned at −70, −50, −30, −20, −15, −10, −5, −1, 0, +1, +5, +10, +15, +20, +30, +50, and +70 mm to the right of the position just under the center of the focal spot.

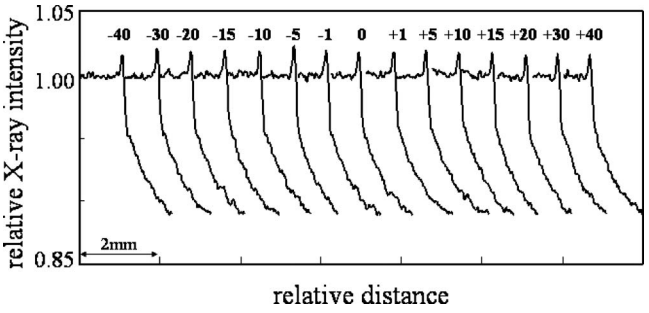

FIG. 17. Profiles obtained by radiography using an acrylic rod. The edge of the acrylic rod was positioned at −40, −30, −20, −15, −10, −5, −1, 0, +1, +5, +10, +15, +20, +30, and +40 mm to the right of the position just under the center of the focal spot.

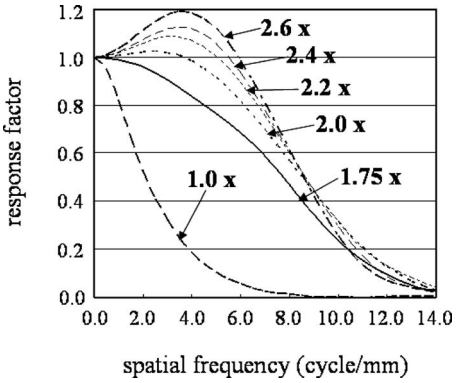

FIG. 19. Response functions by radiography using the acrylic plate with several magnifications.

the horizontal axis correspond with the size of the magnified object. The edges in the profiles before the convolution of the LSF in the S/F system were enhanced clearly irrespective of shapes and sizes of mammary glands. However, the edge enhancements were weakened in the profiles after the convolution of the LSF. Profiles and response functions of 3-mm thick planar mammary-gland edges by PCM and conventional mammography were shown in Fig. 26. Profiles and response functions of 3-mm diametrical cylindrical mammary-gland edges were also shown in Fig. 27. The horizontal axes of the profiles by PCM correspond with the reduced scale to the real size of the object. In the profiles before the convolution of the LSF in Fig. 26, the edge by PCM was enhanced and had sharper slope than that by conventional mammography. Also in the profiles after the convolution, the enhancement and sharper slope by PCM were maintained. Although the edge by PCM was also enhanced in the profiles before the convolution in Fig. 27, the edge slope was not sharper than that by conventional mammography. In the profiles after the convolution, however, the edge by PCM became sharper than that by conventional mammography, though the enhancement was weakened. Ultimately, the response functions by PCM were higher than those by conventional mammography, irrespective of the object shapes. We confirmed same tendency in any size of mammary glands.

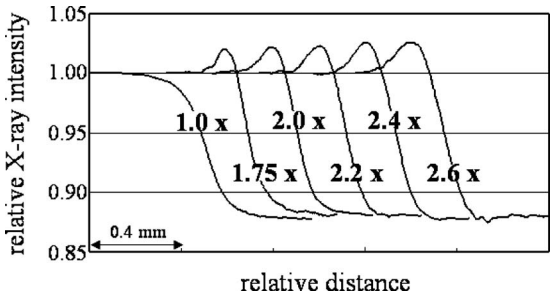

FIG. 18. Profiles by radiography using the acrylic plate with several magnifications.

IV. DISCUSSION

IV.A. MTFs and presampling MTFs

The spatial resolutions in horizontal and vertical directions of the digital camera were equivalent. Thereby, we considered that the difference in MTFs of the S/F system due to the placement directions of the tungsten edge is based on the influences of the incident angles of the x rays into the edge and projected focal spot sizes on the image detector. An oblique incidence of x rays causes a blur on the images and decreases MTFs.[26] At a position 5 cm from the center of the chest wall side of the table, there were many oblique incident x rays in directions (c) and (d) as compared with those along directions (a) and (b). So, MTFs in directions (c) and (d) were lower than those in directions (a) and (b). Additionally, the projected focal spot size on the image detector in directions (a) and (b) would be different from that in directions (c) and (d), although we did not measure respective spot sizes. The larger the focal spot size was, the more the MTF must have been decreased. In the CR system, not only the incident angles of the x rays and projected focal spot sizes but also the scanning directions of the photostimulable phosphor plates also influenced presampling MTFs. Although the results that presampling MTFs for PCM in directions (a) and (b) were higher than those in directions (c) and (d) were opposite to those of presampling MTFs for conventional mammography, the influence of the incident angles of the x rays on the plates must have been the same for PCM and conventional mammography. Hence, the contrastive results between presampling MTFs for PCM and conventional mammography were caused by the influence of the scanning directions of the plates. We confirmed that presampling MTFs in the subscanning direction were higher than those in the main scanning direction in both PCM and conventional mammography. The scanning system may have characteristic cutting signals of a high frequency to remove high-frequency noises and aliasing errors. Although such characteristics of the scanning system interfere with data in the main scanning direction, they do not affect data in the subscanning direction. Consequently, only presampling MTFs in the main scanning direction were affected by these characteristics, and they were lower than those in the subscanning direction. The

reason for presampling MTFs of the CR system for PCM being lower than those for conventional mammography without the adjustment of the spatial frequency could be attributed to the thickness and scanning speed of the plates. It is reasonable to presume that the plates for PCM should be thicker than those for conventional mammography and that the scanning speed of the plate for PCM should be faster than that for conventional mammography. These factors must have influenced the results without the adjustment of the spatial frequency. Nevertheless, presampling MTFs for PCM were increased by the adjustment of the spatial frequency; therefore, we found that the spatial resolution of the plate for PCM was finally improved by the effect of the reduction of the magnified images.

IV.B. Object-edge-response characteristics

As is apparent from Figs. 7 and 8, although the profiles obtained by PCM radiography were enhanced at the edge of the acrylic plate, the intensities of edge enhancements of the profiles changed with the placement directions of the object. The difference in edge enhancements in the S/F system was caused by the incident angles of x rays into the object edge and the projected focal spot sizes on the image detector. At the position 1 cm from the center of the chest wall side of the table, the differences of the angles must be smaller than the difference at the position during MTF measurement. However, we confirmed from the difference in profiles shown in Fig. 7 that the minor difference in the incident angles certainly affected the phenomenon of edge enhancement. Besides, when objects were positioned at 1 cm from the chest wall side, as to directions (c) and (d), the projected focal spot size on the image detector was smaller than the size at the position during MTF measurement. Even so, in the directions with larger projected focal spot of either directions (a) and (b) or directions (c) and (d), the edge profiles must have been more blurred. As a result of these differences by the placement directions, response functions in directions (a) and (b), for which edge enhancements were remarkable, were higher than those in directions (c) and (d). Edge enhancements of profiles caused increases in the response factors in certain bandwidths of spatial frequencies. These bandwidths and intensities of the increases were determined by the widths and intensities of the edge enhancements of the profiles. In the CR system, the difference in edge enhancements due to the placement direction was caused by not only the incident angles of x rays but also the scanning directions of the photostimulable phosphor plates. In directions (a) and (b) in Fig. 8, edge enhancements were remarkable as compared with those in directions (c) and (d) because directions (a) and (b) corresponded to the subscanning direction of the plate and the object-placement directions in which edge enhancements in S/F system were also remarkable. Resultingly, the response functions in directions (a) and (b) were higher than those in directions (c) and (d). We consider that the difference between the response functions for (a) and (b) was influenced by the direction of progress of the subscan of the plate. The subscan progressed along the directions indicated by the double arrows in (a) and (b) in Fig. 8, and it is possible that data scanned later were influenced by the afterglow of the laser-scan beams. Consequently, edge enhancements may have been detected only on the upper side or lower side of the profiles.

From Figs. 9 and 10, we demonstrated that the edge-response characteristics of PCM outperformed those of conventional mammography when either acrylic plate or acrylic rod were used. PCM images must have been blurred by the projected focal-spot blurring, unlike conventional mammograms. Nevertheless, this result was caused by edge enhancements of profiles and the reduction of magnified images. Response functions were increased by edge enhancements, as described previously, and were shifted to high-frequency sides by the reduction of magnified images. The reason why the response function of PCM using the acrylic rod decreased at a low spatial frequency and increased in a spatial frequency range of 2–6 could be attributed to the shape of the object. Further, the fluctuations of the response functions using the acrylic rod may have been caused by noise, although the profiles were averaged. In addition, Fig. 9 shows that the edge-response characteristics in the S/F system were better than those in the CR system. As is apparent from the comparison between the MTFs of the S/F system and the presampling MTFs of the CR system, the spatial resolution of the CR system was worse than that of the S/F system. When low x-ray absorbers such as the acrylic plate were used as the object in the CR system, edge enhancements possibly decreased due to the afterglow of the laser-scan beams, as shown in the profiles in Fig. 8. Eventually, since the intensities of edge enhancements detected in the CR system were lower than those in the S/F system, the edge-response characteristics in the CR system were poorer. Unfortunately, the CR system would have insufficient detection capability to ascertain edge enhancements. However, if the performance of the image detector is improved, for example by optimizing the thickness and scanning speed of the photostimulable phosphor plate, we can expect better edge-response characteristics of PCM in the CR system. Figure 9 also shows that the characteristics of edge response to objects in air were higher than those in oil. From Eqs. (2)–(4), the refractive indexes of air, salad oil, and an acrylic substance were calculated as 0.999 999 998 96, 0.999 999 208 8, and 0.999 998 965 4, respectively, when the energy of x rays was assumed to be 15.5 keV. We considered that these results were obtained because the ratio of the refractive index of air to that of an acrylic substance was larger than that of oil to an acrylic substance.

A comparison of Figs. 7 and 11 reveals that edge enhancements of profiles for which the acrylic rod was used were not remarkable as compared with those for which the acrylic plate was used. Moreover, the edge-response characteristics obtained using the acrylic rod were poorer than those obtained using the acrylic plate. Reportedly, profiles for object edges are enhanced because x rays are refracted at the edges.[11–16] According to the theory of refraction, a larger incident angle of x rays into the object causes a larger refracting angle and more remarkable edge enhancement. Al-

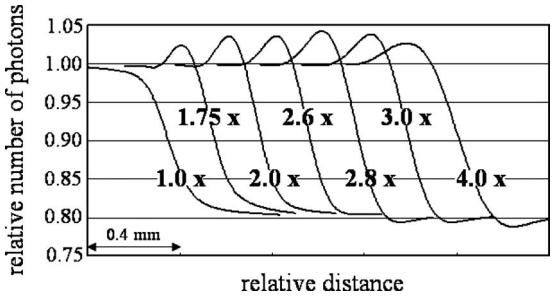

FIG. 20. Profiles by the simulation using the acrylic plate with several magnifications.

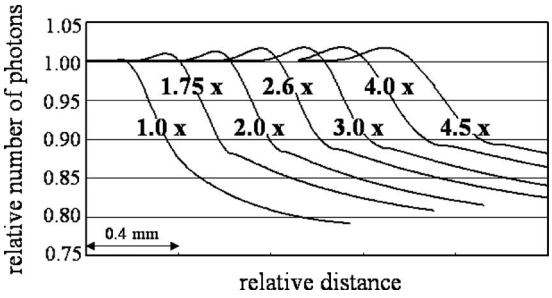

FIG. 22. Profiles by the simulation using the acrylic rod with several magnifications.

though the edge of the acrylic plate is a right angle, that of the acrylic rod is not. Hence, the incident angles of x rays into the side of the edge of the acrylic plate and refracting angles of x rays from the side were larger than those in the case where the acrylic rod was used. Not only the difference in the edge slope by the object shape but also this factor of edge enhancements could have resulted in the edge-response characteristics with the acrylic rod being poorer than those with the acrylic plate. However, in Sec. IV D, we will discuss particularly whether edge enhancements in PCM images can be attributed to the refraction of x rays.

The above results show that the edge-response characteristics of PCM change due to the placement direction of the object, the condition around the object, and the shape of the object. However, irrespective of the object condition, PCM had better characteristics than those of conventional mammography. Moreover, the characteristics of PCM at a high frequency were well maintained as compared with those of conventional mammography. These results revealed that PCM had the ability to resolve the details of object edges.

IV.C. Noise characteristics

The digital Wiener spectral values of the plate for PCM were lower than those for conventional mammography because of the reduction of magnified images. With regard to the distance between the focal spot and the image detector, although this distance in PCM radiography was greater than that in conventional mammography, the attenuation of x rays according to the inverse square law of distance was compensated. This happened because the PCM images were reduced. Since conventional mammography images were obtained with a bucky, scattered x rays and a part of the direct x rays were removed. However, because the PCM images were obtained without a bucky, the direct x rays were not removed. Therefore, we are sure that the amount of x rays that arrive at the image detector in PCM radiography is greater than that in conventional mammography. Not only the effects of the reduction of magnified images but also the difference in the amount of x rays must influence the digital Wiener spectra. The better noise characteristics of the plate for PCM would be effective to diagnose low-contrast breast images.

IV.D. Simulation of refraction of X rays

In profiles obtained by the simulation as well as radiography, when the acrylic plate was used as the object, the forms of the profiles changed according to the position of the object, and the peak intensity of the edge enhancements emerged at about 10-mm position from the position just under the center of the focal spot. That is, the profiles obtained by the simulation behaved almost similarly to how those obtained by radiography did. The simulation was performed under the assumption that the x rays were monochromatic. However, similar changes in the forms of the profiles shown in Fig. 14 were observed at any energy. Therefore, even if polychromatic x rays are used, profiles similar to those in Fig. 14 must be obtained because the profiles of polychro-

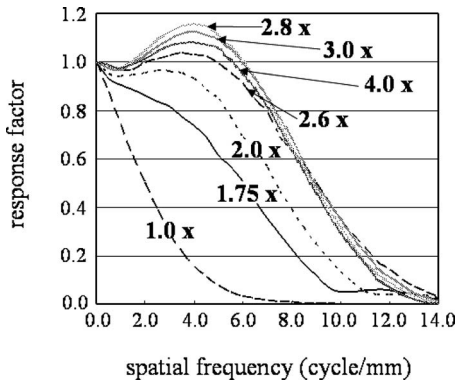

FIG. 21. Response functions by the simulation using the acrylic plate with several magnifications.

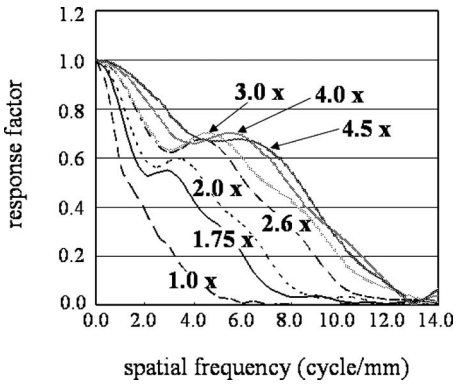

FIG. 23. Response functions by the simulation using the acrylic rod with several magnifications.

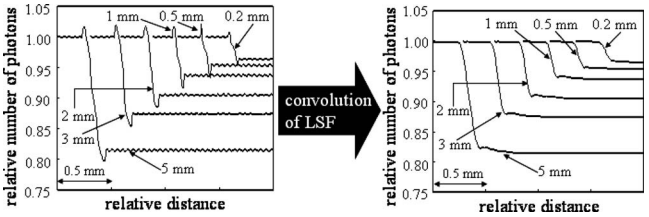

FIG. 24. Profiles of planar mammary-gland edges acquired at a 0.0098-mm pitch by the simulation on the layout of PCM. The left profiles show those before convolution. The right profiles show those after the convolution of the LSF of the S/F system. The thicknesses of the mammary glands were 0.2, 0.5, 1, 2, 3, and 5 mm.

matic x rays are in fact the summations of each monochromatic profile multiplied by the abundance ratio of photons at the respective energies. In other words, even under the assumption that polychromatic x rays are used, the profile behavior obtained by the simulation must be consistent with that obtained by radiography. On the other hand, in profiles obtained by the simulation as well as radiography, the intensities of edge enhancements hardly changed when the acrylic rod was used, irrespective of the object position. Hence, the behavior of profiles obtained by the simulation using the acrylic rod was also consistent with those by radiography.

Figures 28 and 29 show components of profiles by the simulation when the edge of the acrylic plate was positioned at +10 and −10 mm to the right of the position just under the center of the focal spot, respectively. These are profiles before convolution with the LSF. The broken lines in the right panels mean x rays from improbable directions because of the positional relation between the focal spot and the object. Direct x rays that did not contact the object were counted as profile (b). Refracted x rays from upper surface to lower surface of the object were counted as profile (c). Refracted x rays from lateral side to lower surface were counted as profile (d). Refracted x rays from upper surface to lateral side were counted as profile (e). Totally reflected x rays at lateral side were counted as profile (f). Profile (a) shows total of profiles (b), (c), (d), (e), and (f). Figure 28 revealed that edge enhancements were generated by refracted x rays from lateral side to lower side of the acrylic plate when the edge of the object was positioned to the right from under the focal spot. Although a slight distribution by total reflection was detected at −7.56 mm to the right from under the focal spot,

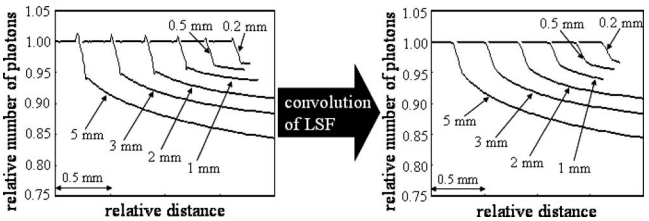

FIG. 25. Profiles of cylindrical mammary-gland edges acquired at a 0.0098-mm pitch by the simulation on the layout of PCM. The left profiles show those before convolution. The right profiles show those after the convolution of the LSF of the S/F system. The diameters of the mammary glands were 0.2, 0.5, 1, 2, 3, and 5 mm.

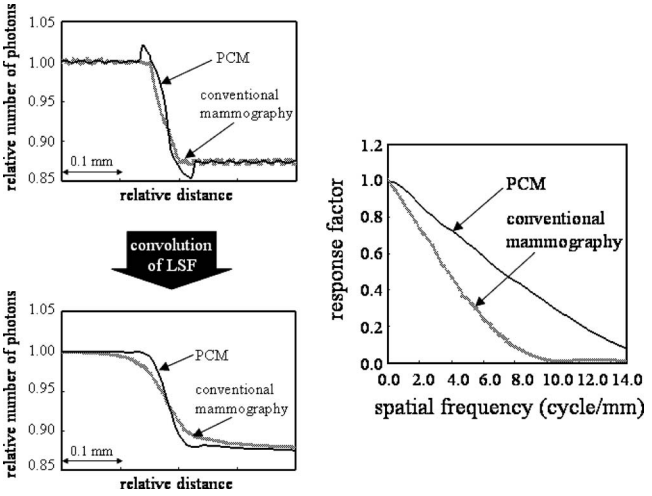

FIG. 26. Profiles and response functions of planar mammary-gland edges of 3 mm thickness by the simulation on the layout of PCM and conventional mammography. The upper left panel shows the profiles before convolution of the LSF, and the lower panel shows those after the convolution. The horizontal axis of the profile by PCM corresponds with the reduced scale to the real size of the object. The right panel shows the response functions calculated from the profiles after the convolution.

the distribution did not contribute to edge enhancements. Figure 29 revealed that edge enhancements were generated by refracted x rays from upper surface to lateral side when the edge was positioned to the left from under the focal spot. A distribution by total reflection was not detected. That is, edge enhancements with a planar object were based on x rays that passed lateral side of the object. Figure 30 shows components of profiles by the simulation when the edge of the acrylic rod was positioned at +10 mm. Direct x rays were counted as profile (b). Refracted x rays in the object were counted as profile (c). Totally reflected x rays at surface of

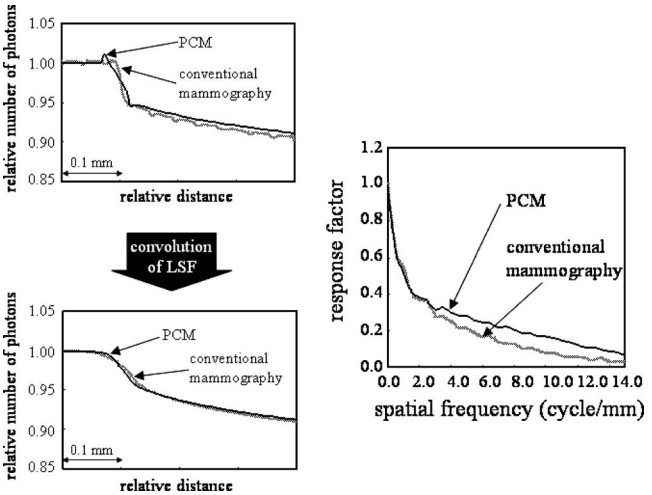

FIG. 27. Profiles and response functions of cylindrical mammary-gland edges of 3-mm diameter by the simulation on the layout of PCM and conventional mammography. The upper left panel shows the profiles before convolution of the LSF, and the lower panel shows those after the convolution. The horizontal axis of the profile by PCM corresponds with the reduced scale to the real size of the object. The right panel shows the response functions calculated from the profiles after the convolution.

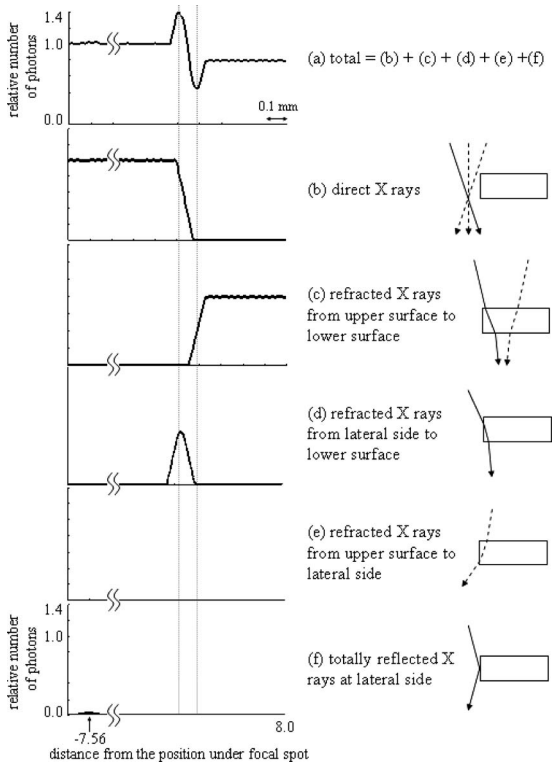

FIG. 28. Components of profiles by the simulation when the edge of the acrylic plate was positioned at +10 mm to the right of the position just under the center of the focal spot. Direct x rays were counted as profile (b). Refracted x rays from upper surface to lower surface of the object were counted as profile (c). Refracted x rays from lateral side to lower surface were counted as profile (d). Refracted x rays from upper surface to lateral side were counted as profile (e). Totally reflected x rays at lateral side were counted as profile (f). Profile (a) shows total of profiles (b), (c), (d), (e), and (f).

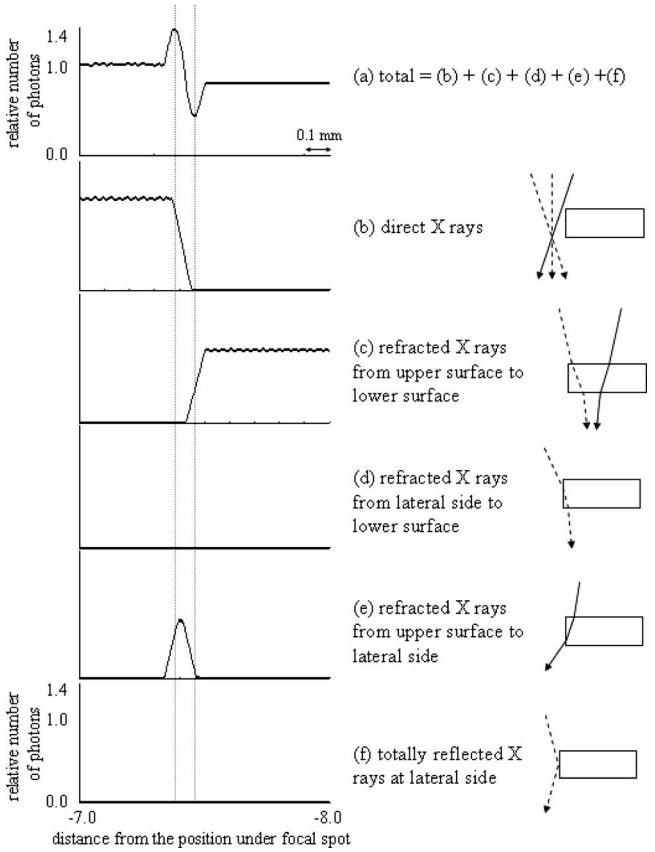

FIG. 29. Components of profiles by the simulation when the edge of the acrylic plate was positioned at −10 mm to the right of the position just under the center of the focal spot. Specifications of each profile are same as those in Fig. 28.

the object were counted as profile (d). Profile (a) shows total of profiles (b), (c), and (d). Although total reflection of x rays occurred barely, the distribution did not converge. So, totally reflected x rays did not contribute to edge enhancements. Similar components were obtained when the edge of the acrylic rod was positioned at −10 mm. It was confirmed that edge enhancements with the acrylic rod were generated by refracted x rays in object. Above results showed that phenomena of edge enhancements in PCM were characterized by the object shapes and the positional relation between the focal spot and the object. However, all edge enhancements by the simulation were based on the refraction of x rays. Accordingly, we verified that edge enhancements in PCM were attributed to the refraction of x rays irrespective of the object shapes, since the behavior of profiles obtained by the simulation was consistent with that obtained by radiography.

IV.E. Phase-contrast effect due to magnification

The results by radiography showed that, as the magnification was increased within the range between 1.75 and 2.6, response characteristics were more improved. As the magnification is increased, shifts of projected positions to the image detectors by refraction of x rays must be larger. The increments of the shifts of projected positions would result in more enhanced edge profiles and better response characteristics. The simulated results using the acrylic plate showed that response characteristics were best with the magnification about 3.0, and the results using the acrylic rod showed that the characteristics were best with 3.0 or 4.0. If the magnification is increased, although the shifts of projected positions must be larger, the focal-spot blurring becomes also more influential. The effects of the shifts of projected positions would have been dominant with the magnification less than 3.0 (or 4.0), while the focal-spot blurring would have been influential with that not less than 3.0 (or 4.0).

The comprehensive results suggested that the magnification about 3.0 may be more suitable for PCM than 1.75 in the commercialized system, when the FID is 1140 mm. Noise characteristics are theoretically invariable with any magnification if magnified images are reduced to the real size of the object. However, our simulation was performed under particular-object conditions because the objects were acrylic substances in air and the shapes were planar or cylindrical. Therefore, the optimal magnification for PCM could not be decided from only our results. The decision of the optimal magnification would be difficult, since wide-scale image detectors are needed if the magnification is increased.

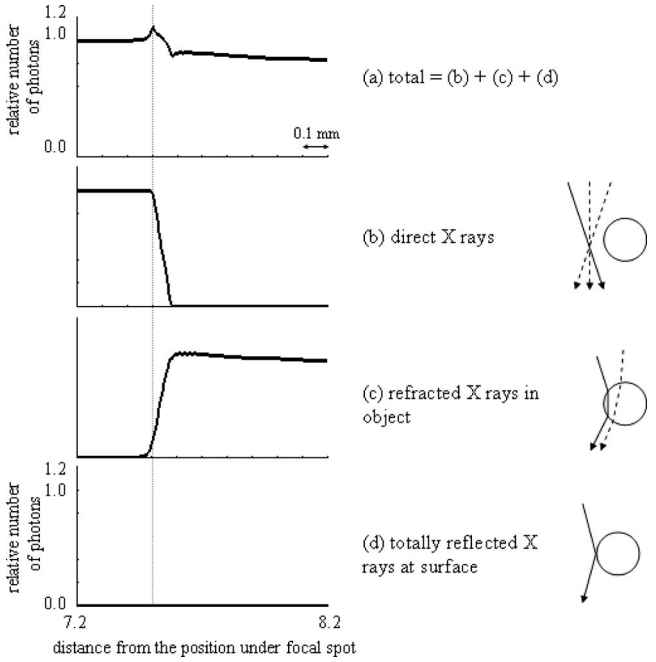

FIG. 30. Components of profiles by the simulation when the edge of the acrylic rod was positioned at +10 mm to the right of the position just under the center of the focal spot. Direct x rays were counted as profile (b). Refracted x rays in the object were counted as profile (c). Totally reflected x rays at surface of the object were counted as profile (d). Profile (a) shows total of profiles (b), (c), and (d).

Nevertheless, we proposed that larger magnification than 1.75 in the commercialized system might be more suitable for PCM.

IV.F. Phase-contrast effect to breast tissue

Our simulated results before the convolution of the LSF in the S/F system showed that edge enhancements occurred certainly at edges of mammary glands in adipose tissue irrespective of shapes and sizes of mammary glands. Although the edge enhancements were weakened by the image-detector blurring in the S/F system, the enhancements were maintained even after the convolution so that the edges by PCM were sharper than those by conventional mammography. Because the edge portions on the profiles by PCM were dragged by the enhancements, the profiles were less blurred than those by conventional mammography. That is why edge slopes by PCM and conventional mammography in the cylindrical edge profiles were reversed between before and after the convolution. Eventually, we confirmed that the edge-response characteristics at mammary glands in adipose tissue by PCM were better than those by conventional mammography. These results were caused by not only the inherent edge enhancements but also the reduction of magnified images. However, note that these profiles were acquired from counting photons at a pitch of 0.0098 mm and were convoluted by the LSF in the S/F system, though PCM images are sampled at a 0.04375-mm pitch by the CR system in the commercialized system. In fact, the edge enhancement in the commercialized system would be more blurred and the response characteristics would be lower than those shown in Figs. 24–27. Even so, the inherent edge enhancements and the reduction of magnified images may also help the improvements of response characteristics of the commercialized PCM.

Table II shows that densities and linear attenuations of mammary gland and breast carcinoma are similar values. That is, similar results are expected if breast carcinoma in adipose tissue is presumed. Furthermore, because the ratio of the refractive index of adipose tissue to that of calcification was larger than that of adipose tissue to mammary gland, we can expect larger intensities of edge enhancements than those of mammary gland, if calcification in adipose tissue is presumed. So, PCM has better edge-response characteristics than those of conventional mammography even if the object is breast tissues. This ability would enable the clear representation of edges of structures such as mammary glands, breast carcinomas, and microcalcifications in mammograms. As already described in Sec. IV C, noise characteristics of PCM were better than those of conventional mammography because of the reduction of magnified images and the effects without a bucky. Ultimately, PCM would be effective in the diagnoses of breast images.

V. CONCLUSION

We measured the physical image characteristics of PCM and conventional mammography. The influences of phase contrast on x-ray images were measurable, since the edge-response characteristics were measured using acrylic substances as objects. We revealed that the edge-response characteristics of PCM outperformed those of conventional mammography because of edge enhancements and the reduction of magnified images. It was confirmed that PCM had better noise characteristics than those of conventional mammography. The results of our simulation showed that edge enhancements in PCM depended on the object shapes and the positional relation between the focal spot and the object. Furthermore, we demonstrated that the edge enhancements are attributed to the refraction of x rays irrespective of the object shapes. We also proposed that larger magnification than 1.75 in the commercialized system might be more suitable for PCM. Our investigation of phase-contrast effects to breast tissues suggested a possibility that PCM would be helpful in the diagnoses of breast images.

ACKNOWLEDGMENTS

The authors are grateful to Dr. Chika Honda, Hiromu Ohara, Junko Kiyohara, and Kazuhiro Kido of Konica Minolta M&G, Inc. for their helpful advice and useful discussions.

[a]Current address: Osaka General Medical Center, 3-1-56 Mandaihigashi, Sumiyoshi-Ku, Osaka, Japan 558-8558; Electronic mail: asumintgreen_0124@yahoo.co.jp

[1]A. Momose and J. Fukuda, "Phase-contrast radiographs of nonstained rat cerebellar specimen," Med. Phys. **22**, 375–379 (1995).
[2]R. E. Johnston, D. Washburn, E. Pisano, C. Burns, W. C. Thomlinson, L. D. Chapman, F. Arfelli, N. F. Gmur, Z. Zhong, and D. Sayers, "Mammographic phantom studies with synchrotron radiation," Radiology **200**,

659–663 (1996).
[3]S. W. Wilkins, T. E. Gureyev, D. Gao, A. Pogany, and A. W. Stevenson, "Phase-contrast imaging using polychromatic hard x rays," Nature (London) **384**, 335–338 (1996).
[4]N. Yagi, Y. Suzuki, and K. Umetani, "Refraction-enhanced x-ray imaging of mouse lung using synchrotron radiation source," Med. Phys. **26**, 2190–2193 (1999).
[5]R. Fitzgerald, "Phase-sensitive x-ray imaging," Phys. Today **53**, 23–26 (2000).
[6]P. Monnin, S. Bulling, J. Hoszowska, J. F. Valley, R. Meuli, and F. R. Verdun, "Quantitative characterization of edge enhancement in phase contrast x-ray imaging," Med. Phys. **31**, 1372–1383 (2004).
[7]M. Hirano, K. Yamasaki, H. Okada, T. Sakurai, T. Kondoh, T. Katafuchi, K. Sugimura, S. Kitazawa, R. Kitazawa, S. Maeda, and S. Tamura, "Ray tracing analysis of overlapping objects in refraction contrast imaging," Radiol. Med. (Torino) **23**, 386–389 (2005).
[8]X. Wu and H. Liu, "Clinical implementation of x-ray phase-contrast imaging: Theoretical foundations and design considerations," Med. Phys. **30**, 2169–2179 (2003).
[9]X. Wu and H. Liu, "A new theory of phase-contrast x-ray imaging based on Wigner distributions," Med. Phys. **31**, 2378–2384 (2004).
[10]C. J. Kotre and I. P. Birch, "Phase contrast enhancement of x-ray mammography: A design study," Phys. Med. Biol. **44**, 2853–2866 (1999).
[11]T. Tanaka, C. Honda, S. Matsuo, K. Noma, H. Ohara, N. Nitta, S. Ota, K. Tsuchiya, Y. Sakashita, A. Yamada, M. Yamasaki, A. Furukawa, M. Takahashi, and K. Murata, "The first trial of phase contrast imaging for digital full-field mammography using a practical molybdenum x-ray tube," Invest. Radiol. **40**, 385–396 (2005).
[12]H. Ohara, C. Honda, A. Ishisaka, and F. Shimada, "The improvement of x-ray image sharpness in x-ray phase imaging," Konica Minolta Technology Report **1**, 131–134 (2004).
[13]T. Gido, S. Nagatsuka, K. Amitani, H. Yonekawa, M. Shimoji, and C. Honda, "Advanced digital mammography system based on phase contrast technology," Proc. SPIE **5745**, 511–518 (2005).
[14]S. Matsuo, T. Katafuchi, K. Tohyama, J. Morishita, K. Yamada, and H. Fujita, "Evaluation of edge effect due to phase contrast imaging for mammography," Med. Phys. **32**, 2690–2697 (2005).
[15]A. Ishisaka, H. Ohara, and C. Honda, "A new method of analyzing edge effect in phase contrast imaging with incoherent x rays," Opt. Rev. **7**, 566–572 (2000).
[16]A. Ishisaka, H. Ohara, C. Honda, and F. Shimada, "Theoretical analysis of phase contrast imaging for mammography," Konica Minolta Technology Report **2**, 31–33 (2005).
[17]IEC 62220-1-2, "Medical electrical equipment-characteristics of digital x-ray imaging devices—Part 1: Determination of the detective quantum efficiency, Section 2: Detectors used in mammography," 2005, pp. 3–33.
[18]K. Ichikawa, H. Fujita, and T. Sawada, "Novel MTF measurement method for medical image viewers using a bar pattern image," Proc. SPIE **5029**, 624–631 (2003).
[19]A. Horii, A. Chihara, K. Ichikawa, Y. Kodera, M. Ikeda, and T. Ishigaki, "Measurement of modulation transfer functions for liquid crystal displays by rectangular waveform analysis," Jpn. J. Radiol. Technol. **61**, 1651–1655 (2005).
[20]A. Horii, M. Takamura, K. Ichikawa, Y. Kodera, M. Ikeda, and T. Ishigaki, "Measurement of MTFs for monochrome and color liquid crystal displays," Proc. SPIE **6141**, 61411P–61419P (2006).
[21]K. Ichikawa, Y. Kodera, and A. Horii, "Novel NPS measurement method for medical liquid crystal display using periodic components subtraction technique," Proc. SPIE **6142**, 61423H–61431H (2006).
[22]K. Ichikawa, Y. Kodera, and H. Fujita, "MTF measurement method for medical displays by using bar-pattern images," SID J. **14**, 831–837 (2006).
[23]B. L. Henke, E. M. Gullikson, and J. C. Davis, "X-ray interactions: Photoabsorption, scattering, transmission, and reflection at $E=50-30{,}000$ eV, $Z=1-92$," At. Data Nucl. Data Tables **54**, 181–342 (1993).
[24]L. G. Parratt, "Surface studies of solids by total reflection of x-rays," Phys. Rev. **95**, 359–369 (1954).
[25]F. Maeda, A. Ogura, and A. Miyai, "Signal detectability of mammography depends on film-screen system and luminance of view box," Jpn. J. Radiol. Technol. **59**, 746–750 (2003).
[26]J. G. Mainprize, A. K. Bloomquist, M. P. Kempston, and M. J. Yaffe, "Resolution at oblique incidence angles of a flat panel imager for breast tomosynthesis," Med. Phys. **33**, 3159–3164 (2006).